EBioMedicine 73 (2021) 103670

Contents lists available at ScienceDirect

EBioMedicine

journal homepage: www.elsevier.com/locate/ebiom

Research Article

Resolving immune cells with patrolling behaviour by magnetic resonance time-lapse single cell tracking

Max Masthoff[a,*], Felix Noah Freppon[a], Lisa Zondler[b], Enrica Wilken[a], Lydia Wachsmuth[a], Silke Niemann[c], Christian Schwarz[a], Ina Fredrich[a], Asli Havlas[a], Helena Block[b], Mirjam Gerwing[a], Anne Helfen[a], Walter Heindel[a], Alexander Zarbock[b], Moritz Wildgruber[a,d,†], Cornelius Faber[a,†]

[a] Clinic for Radiology, Translational Research Imaging Centre, University Hospital Muenster, Muenster, Germany
[b] Department of Anaesthesiology, Intensive Care and Pain Medicine, University Hospital Muenster, Muenster, Germany
[c] Institute of Medical Microbiology, University Hospital of Muenster, Muenster, Germany
[d] Department of Radiology, University Hospital, LMU Munich, Munich, Germany

ARTICLE INFO

Article History:
Received 5 August 2021
Revised 10 October 2021
Accepted 19 October 2021
Available online xxx

Key words:
patrolling monocytes
time-lapse MRI
single cell tracking
immune response
iron oxide nanoparticles

ABSTRACT

Background: Immune cells show distinct motion patterns that change upon inflammatory stimuli. Monocytes patrol the vasculature to screen for pathogens, thereby exerting an early task of innate immunity. Here, we aimed to non-invasively analyse single patrolling monocyte behaviour upon inflammatory stimuli.
Methods: We used time-lapse Magnetic Resonance Imaging (MRI) of the murine brain to dynamically track single patrolling monocytes within the circulation distant to the actual site of inflammation in different inflammatory conditions, ranging from a subcutaneous pellet model to severe peritonitis and bacteraemia.
Findings: Single patrolling immune cells with a velocity of <1 μm/s could be detected and followed dynamically using time-lapse MRI. We show, that due to local and systemic stimuli the slowly patrolling behaviour of monocytes is altered systemically and differs with type, duration and strength of the underlying stimulus.
Interpretation: Using time-lapse MRI, it is now possible to investigate the behaviour of single circulating monocytes over the course of the systemic immune response. Monocyte patrolling behaviour is altered systemically even before the onset of clinical symptoms distant to and depending on the underlying inflammatory stimulus.
Funding: This study was supported by the Deutsche Forschungsgemeinschaft (DFG, German Research Foundation) - CRC 1009 - 194468054 to AZ, CF and - CRC 1450 - 431460824 to MM, SN, HB, AZ, CF, the Joachim Herz Foundation (Add-on Fellowship for Interdisciplinary Life Sciences to MM), the Interdisciplinary Centre for Clinical Research (IZKF, core unit PIX) and the Medical Faculty of the University of Muenster (MEDK fellowship to FF and IF).

1. Introduction

Inflammation triggers a systemic response by the innate and adaptive immune system. This response drives the development, manifestation and extent of disease and is modulated by the underlying inflammatory stimulus ranging from local tissue damage to systemic infection. The immune response is particularly strong during sepsis, which is defined by a dysregulated host immune response [1]. Moreover, immune cell behaviour and interplay within the tumour microenvironment play a crucial role in cancer progression and development of metastasis [2-4]. Immune cells change their motion pattern upon inflammatory insults, and then typically exert a rolling behaviour, which represents an important step of leucocytes extravasating the vasculature to sites of inflammation [5-7]. In contrast, under healthy conditions a slower patrolling behaviour of non-classical monocytes has been described, with the cells screening the endothelium in loop, hairpin or wave-shaped pathways at a velocity of 0.2 μm/s [5]. Such patrolling behaviour lasts for varying durations and has been described being either restricted to small regions (diameter <40 μm) or extended over longer distances (>100 μm). Currently, observation of patrolling and rolling monocytes requires invasive techniques such as intravital microscopy (IVM) [5,8]. This imaging method only provides a very limited field of view and disrupts the integrity of the organism potentially activating the

* Correspondence should be addressed to M M
E-mail address: max.masthoff@ukmuenster.de (M. Masthoff).
† These authors contributed equally

https://doi.org/10.1016/j.ebiom.2021.103670

Research in context

Evidence before this study

Intravascular immune cells screen the endothelium for pathogens in a healthy state (so called patrolling) while upon inflammatory stimuli these cells start rolling on the endothelium aiming to leave the vasculature at the site of inflammation, which is modulated by the leucocyte adhesion cascade. Currently, these dynamic processes can only be imaged by means of invasive methods such as intravital microscopy. Further, knowledge about motion behaviour of immune cells distant to the site of the inflamed vascular bed is scarce.

Added value of this study

In this work, we established a technique to non-invasively detect and dynamically follow single intravascular patrolling immune cells using repeated time-lapse magnetic resonance imaging. This enabled to study the patrolling behaviour of immune cells non-invasively and even distant to the stimulus in different inflammatory conditions ranging from local inflammation to severe systemic sepsis. Thereby, this work shows that patrolling behaviour of immune cells is altered systemically even before the onset of clinical symptoms and differs with type, duration and strength of the underlying stimulus.

Implications of all the available evidence

It is now possible to non-invasively study the behaviour of single circulating immune cells in response to inflammatory stimuli, which is a valuable tool for preclinical research and may perspectively become a diagnostic clinical surrogate marker for inflammatory diseases.

organisms' host-defence system. Both limitations impair the characterization of systemic immune cell dynamics, in particular with regards to clinical translation. Knowledge about onset, type and extent of the intravascular motion pattern of immune cells in response to inflammatory triggers and/or in steady state remains scarce, especially for patrolling immune cells distant from the inflammatory site. Until the concept of time-lapse MRI was implemented [9,10], actual movement of single cells remained concealed for non-invasive imaging. Earlier studies had displayed single cells at different locations or time points, but did not capture intravascular motion [11-14]. The implementation of time-lapse MRI enabled to non-invasively depict slow motion of individual labelled monocytes, while fast moving cells were beyond the detection range [9,10]. Time-lapse MRI, thus appears to be a promising tool for detecting and characterizing patrolling monocytes. Since it provides a non-invasive view of the entire brain with a spatial in-plane resolution between 50 and 100 μm, it may even distinguish short-range from long-range patrolling monocytes.

This study aims to resolve and study patrolling monocyte motion patterns within the circulation in healthy mice and upon different local or systemic inflammatory stimuli by time-lapse MR imaging. We envision to establish the technique as non-invasive single cell-based imaging surrogate for the onset of systemic immune response.

2. Methods

2.1. Animals and Ethics

Animal husbandry and experiments were carried out according to local animal welfare guidelines and were approved by local authorities (ID: 84-02.04.2017.A095, 81-02.04.2019.A004, 84-02.04.2014.A073). Female C57BL/6 mice were obtained from Charles River Laboratories (Sulzfeld, Germany), LysM-GFP mice (GFP expression in myeloid cells, expression level dependent on cell type [15] were obtained from the faculty's animal facility (Münster, Germany). Mice were housed under a 12 h light−dark cycle and provided with food and water ad libitum. Mice were monitored daily for disease symptoms.

2.2. MRI

Ferucarbotran (diameter 50-100 nm, Resovist®, Bayer AG, Germany), approved standard iron oxide nanoparticles (ION)) or rhodamine-conjugated ION (diameter 100 nm diameter; nano-screen MAG-DEAE, Chemicell GmbH, Berlin, Germany), were used as MRI contrast for *in vivo* labelling by injection of 1.9 ml per kg body weight (=53.2 mg Fe per kg bodyweight) i.v. via the tail vein.

Time-lapse MRI of the brain was performed on a 9.4 T Biospec (Bruker Biospin, Ettlingen, Germany) using a cryogenic probe as recently described [9]. Here, a T2* gradient echo sequence with the following scan parameters was applied: TR: 649 ms, TE: 8.0 ms, FA: 60°, averages: 4, matrix: 180 x 256, in-plane resolution: 61 x 55 μm^2, 38 contiguous slices, slice thickness: 300 μm, scan time: 8 min 12 s (single time frame) resulting in 2 h 44 min for 20 repetitions. Mice were anesthetized with 1-1.5% isoflurane in 1 L per minute of oxygen and compressed air (20:80) under continuous respiratory and temperature monitoring. To avoid body cooling, mice were kept at physiologic temperature by a custom-designed animal heating device. Pronounced reduction of body temperature or breathing frequency despite lowering of anaesthetic dose was stop criteria for the measurements. Data was discarded and no time-lapse MRI data analysis was performed under such unstable conditions.

For *in vitro* phantom studies 2 ml agarose gel phantoms (1%) were created without supplement of iron oxide particles (control) or with addition of either 1) Compel™ particles (mean diameter 8.2 μm, 9.2 pg iron per particle, 1000 particles/ml, 9.2 x 10^{-6} mg Fe/ml), 2) ProMAG® particles (mean diameter 2.75 μm, 2.7 pg iron per particle, 1000 particles/ml, 2.3 x 10^{-6} mg Fe/ml) or 3) Resovist® (Ferucarbotran, diameter 50-100 nm, 2.4 x 10^{13} particles/ml, 2.3 x 10^{-6} mg Fe/ml) and examined with the same time-lapse MRI sequence as described above.

2.3. Models of Inflammation

We observed the patrolling behaviour of monocytes within the brain (distant to the site of inflammation) using three inflammatory settings mimicking common clinical situations ranging from peripheral sterile stimuli, bacteraemia to peritonitis following visceral hollow organ perforation.

2.3.1. Peripheral stimulus by subcutaneous inflammation

The "local" model comprised a sterile, peripheral inflammation caused by local subcutaneous injection of polyacrylamide-gel containing lipopolysaccharides (LPS; pellet model). A scheme of experimental setup is represented in Figure 1a. A localized sterile inflammation was induced by subcutaneous injection of 100 μl polyacrylamide gel (PAG) each in both flanks of C57BL/6 mice as previously described [16-18]. To modify the strength of inflammatory stimulus PAG was mixed with either 10 μg or 40 μg of lipopolysaccharide (LPS; n = 6 each). 24h after pellet application Ferucarbotran ION (1.9 ml per kg/body weight) were injected i.v. for *in vivo* labelling of immune cells. Time-lapse MRI of the brain was performed 48 h after pellet application. Additionally, to evaluate immune cell dynamics over the time course of the inflammatory stimulus, Ferucarbotran ION (1.9 ml per kg/body weight) were injected i.v. either 3 h (n = 6), 24 h (n = 6), 48 h (n = 5), 6 d (n=5) or 29 d (n = 5) after pellet

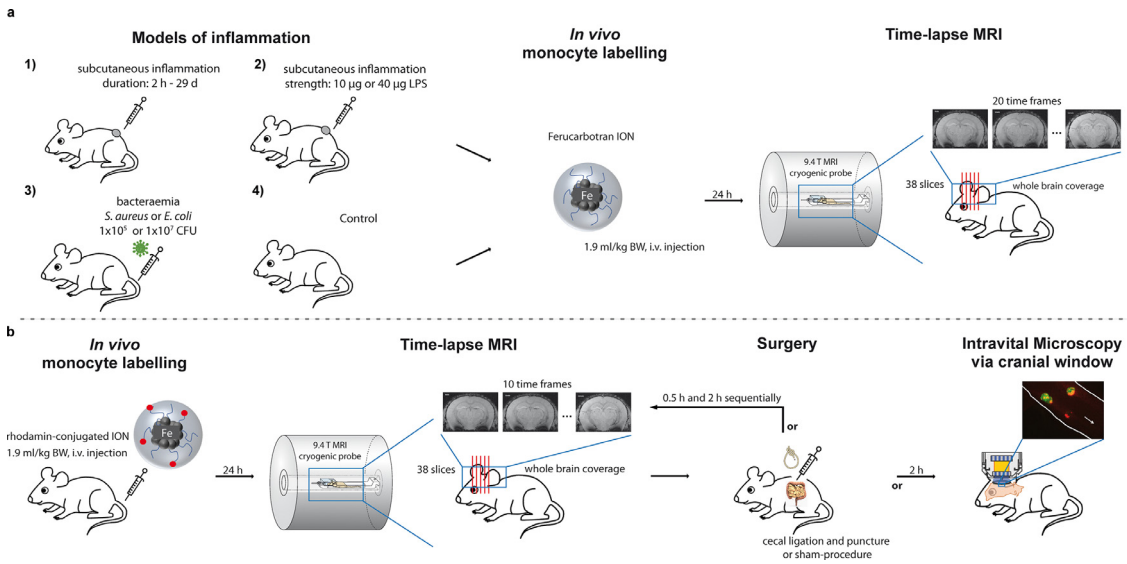

Figure 1. Animal models to study patrolling behaviour of monocytes a) Peripheral sterile inflammation ("local" model) was caused by subcutaneous injection of polyacrylamide-gel (PAG) containing lipopolysaccharides (LPS). Time-lapse MRI was performed 24h after *in vivo* labelling with iron-oxide nanoparticles (ION, Ferucarbotran) either at 5 time-points ranging from 2h to 29d after PAG application (at least n = 5 each; number 1) or after modulating the LPS dose (n=6 each, number 2). Besides, "systemic intravascular" stimulus was induced by bacteraemia using gram-positive (*S. aureus*) or gram-negative (*E. coli*) bacterial strains with varying dose (number 3) followed by *in vivo* labelling of monocytes with iron-oxide nanoparticles (ION, Ferucarbotran). Healthy mice served as control (number 4). For number 1 to 4 time-lapse MRI was performed 24 h after in vivo labelling within a 9.4 T small animal MRI with cryogenic probe using a time-lapse MRI sequence with whole brain coverage and 20 time-frames. **b)** Additionally, a "systemic extravascular" stimulus was induced by an iatrogenic hollow organ perforation via cecal ligation and puncture (CLP) causing massive peritonitis. Time-lapse MRI was performed longitudinally 24 h after *in vivo* labelling with rhodamine-conjugated ION prior to and 0.5 h and 2 h after CLP (n = 4) or sham surgery (n = 3), respectively. Additionally, intravital microscopy via a cranial window was performed 2 h after CLP or sham surgery of mice (n = 3-4). Healthy mice served as control.

application (100 μl PAG per flank mixed with 10 μg LPS) followed by time-lapse MRI of the brain 24 h later. The immune response in the pellet model is known to evolve during one week, peaking at day 3-7 after induction, and to subside beyond day 7 [16,18]. Control mice (n = 8) with no pellet application received time-lapse MRI 24 h after ION injection, similarly. Time-lapse MRI of the brain was performed using 20 repeated time frames.

2.3.2. Systemic intravascular stimulus by bacteraemia

The "systemic intravascular" model consisted of a systemic intravascular stimulus by bacteraemia. A scheme of experimental setup is depicted in Figure 1a. To evaluate immune cell dynamics in response to different systemic bacterial stimuli, both gram-positive (*S. aureus* Newman) or gram-negative (*E. coli* ATCC25922) bacteria were used in this model. Either 1 x 10^5 or 1 x 10^7 colony forming units (CFU) of *S. aureus* Newman or *E. coli* ATCC25922 in 100 μl PBS were injected i.v. in the tail vein of C57BL/6 mice (n = 4 each). 24 h after bacterial injection, Ferucarbotran ION (1.9 ml per kg/body weight) were injected i.v. for *in vivo* labelling of immune cells. Time-lapse MRI of the brain was performed 48 h after bacterial injection. Control mice (n = 8) with no bacteria injection received time-lapse MRI 24 h after ION injection. Time-lapse MRI of the brain was performed using 20 time frames. After time-lapse MRI blood samples were obtained by cardiac puncture under deep anaesthesia before mice were sacrificed.

2.3.3. Systemic extravascular stimulus by hollow organ perforation

The "systemic extravascular" model of inflammation consisted of a systemic extravascular visceral stimulus achieved by (iatrogenic) hollow organ perforation leading to severe peritonitis. A scheme of experimental setup is represented in Figure 1b. This was accomplished by an established model of cecal ligation and puncture (CLP) surgery as previously described [19]. 24 h after intravenous injection of rhodamine-conjugated ION (53.2 mg Fe/kg body weight (bw)) for *in vivo* labelling the surgery procedure was performed. Due to difference in size of rhodamine-ION (100 nm) compared to clinically approved Ferucarbotran ION, increase in detected cells was expected due to higher *in vivo* uptake by monocytes. Briefly, mice were anesthetized by intraperitoneal injection of ketamine (100 μg/g bw) and xylazine (10 μg/g bw). The abdomen was shaved, disinfected by application of 70% ethanol and the mice were placed on a heating pad at 37°C. Next, the abdomen and the peritoneum were opened with sterilized scissors by ~1 cm laparotomy. The cecum was exposed, the distal third was ligated using a sterile silk suture and punctured using a 30G needle. The cecum was replaced into the abdominal cavity. In case of sham operation, no cecal ligation was performed. The peritoneum was closed using 6G silk sutures and the abdomen was closed by careful application of fibrin glue (3M Vetbond).

Prior to (as control), as well as after sham (n = 3) or CLP (n = 4) surgery, anaesthesia was continued with 1-1.5% isoflurane in 1 L per minute of oxygen and compressed air (20:80) and mice were immediately transferred to repeated time-lapse MRI (0.5h and 2h after surgery), which was performed with 10 time-frames each using the same time-lapse MRI sequence. Another n = 3 mice per group did receive intravital microscopy via a cranial window 2 h post-surgery instead of MRI to detect rhodamine-ION labelled cells. In CLP mice symptoms of peritonitis soar about 6h after the surgical procedure and evolve to severe sepsis within 24h. Mice were sacrificed after last time-lapse MRI or IVM scan (about 30h post ION application), respectively. Here, blood samples were obtained by cardiac puncture and were analysed by FACS to assess cell labelling efficacy.

2.4. Cortex Intravital Microscopy

Cortex intravital microscopy (IVM) was performed as previously described by Jenne et al. [20]. Briefly, mice were anaesthetised by intraperitoneal injection with ketamine (100 μg/g bw + xylazine (10 μg/g bw)), placed on a heating pad to control the body temperature and fixed in a custom-made stereotactic frame. The skin was sterilized by 70% ethanol, opened and the periosteum was removed using a scalpel. The skull was opened to create a cranial window

using a drill and removed using regular fine forceps (LST). Next a rubber ring (6 mm diameter; conventional hardware store) was carefully installed and fixed with fibrin glue (3M Vetbond) on the skull surrounding the cranial window to stabilize a droplet of prewarmed PBS (PAN Biotech), which was used to moisturize the tissue and to keep the conditions as physiologic as possible. Spinning disc microscopy was performed on an upright spinning disc confocal microscope (CellObserver SD, Zeiss, Germany) equipped with a HXP120c + LSM T-PMT lighting unit and FLUAR water immersion objectives (10x, 63x were used). The body temperature and depth of anaesthesia of the mice were constantly controlled. Images and movies were acquired using the ZEN software (Zeiss, Germany). Quantification of cell velocities was performed using ImageJ 1.53a (Wayne Rasband, National Institute of Health, USA).

2.5. Flow cytometry

100 μl blood was drawn from the facial vein, erythrocytes were lysed using ACK lysis buffer (150 mM NH4Cl; 10 mM KHCO3; 0,1 mM Na2EDTA) for 8 min at room temperature, centrifuged at 500 x g for 5 min, washed in PBS and transferred to FACS tubes. Flow cytometry was performed on a BD FACSCantoTM II Cell Analyzer, the FITC and PerCP-Cy5.5 channels were used to determine GFP and rhodamine fluorescence.

2.6. Analysis of MRI data

MRI data were processed using Matlab (The MathWorks, Inc., Natick, MA) and ImageJ (Version 1.50b, Wayne Rasband, National Institute of Health, USA). Hypointense spots representing labelled cells were manually counted and matched in all acquired slices and time frames of the brain. Hence, primary outcome measure was number of detected cells by time-lapse MRI. Subsequently, motion patterns of detected cells were subcategorised in short-term (cells detected in one or two consecutive time frames), long-term short-range (cells detected in three or more consecutive time frames) or long-term long-range (cells detected in three or more consecutive time frames with observed motion in-plane or to a consecutive slice) pattern.

We performed Matlab computer simulations to determine the velocity range of cells detectable by time-lapse MRI, as previously described(9). Briefly, synthetic iron-labelled cells were added by 4 voxel signal voids at random positions to the synthetic phantom (intensity = 1, size of 180 by 256 voxels). Here, the intensity in the central voxel of the signal void was reduced to 0.5, and neighbouring voxels to 0.7 comparable to signal intensity loss observed in *in vivo* data. Diagonal motion of the artificial cell was stepwise increased within the synthetic k space, thus simulating different motion velocities by assembling different fractions of position-specific k space data. Image reconstruction was performed by Fourier transformation as previously described(9). Additionally, an overlay of acquired time-lapse MRI data and simulations was realized by a voxel-wise multiplication of the two images. The resulting images not only account for noise, anatomical structures, and imaging artefacts but also allow a direct comparison between real iron-labelled and artificial cells.

2.7. Statistics

Figures were produced using GraphPad Prism version 4.0 (GraphPad Software, San Diego, USA) and Adobe Illustrator CS3 (Adobe, San Jose, USA). Raters of MRI data were blinded for associated experimental group. Sample size determination was performed according to animal welfare guidelines of the local authorities. Mice were allocated at random to treatment or control group and were otherwise treated equally to avoid potential confounders. Exclusion criteria for time-lapse MRI data were unstable animal conditions prior to acquisition of time-lapse MRI dataset as described in detail above. Besides, no data was excluded. Statistical analysis was performed with SPSS version 27 (IBM, Armonk, USA). Results shown are means and standard error of the mean. Welch-ANOVA with Games-Howell post-hoc test or Tukey post-hoc test (depending on homogeneity of variances as asserted by Levene's Test) was performed for grouped analysis. Repeated measures(rm-) ANOVA with Bonferroni-adjusted post-hoc analysis was performed to analyse paired data. Here, if violations of sphericity occurred as indicated by the Mauchly test, the Greenhouse–Geisser adjustment was used. P-values <0.05 were considered statistically significant. The raw data of the study are available from the corresponding author on reasonable request.

2.8. Role of funding sources

The bodies funding this study had no role in the design, data collection, data analyses, interpretation or the writing of the report.

3. Results

3.1. Resolving patrolling monocytes by time-lapse MRI

To characterize the motion patterns of slowly moving immune cells (Figure 2a), we first verified that time-lapse MRI allows for detecting single patrolling monocytes. For this purpose, we implemented *in vivo* time-lapse MRI with an 8-minute temporal resolution per time-frame and 61 μm by 55 μm in-plane resolution, covering the entire mouse brain. Time-lapse MRI consists of repeated acquisition of this sequence for video-like cell tracking. To assess a relevant contribution of free iron oxide nanoparticles to the observed signal changes, we performed *in vitro* phantom measurements (supplementary Figure 1). Only iron particles with a diameter in the μm range resulted in observable hypointensities but not the ION with a diameter of 50-100 nm used *in vivo* within this study. Together with the expected high motion velocities of free ION in the blood stream, the phantom measurements lead to the conclusion that a relevant contribution of free particles to MRI signal was most unlikely. Further, the phantom measurements showed that the time-lapse MRI sequence was capable of detecting hypointensities caused by an amount of $>$2.5 pg Fe/particle, an amount of iron which has previously been reached by labelling monocytes with ION [9]. We therefore conclude, that signal hypointensities observed by time-lapse MRI can be attributed to single cells. We determined the number of intravascularly moving monocytes labelled *in vivo* via phagocytosis with iron oxide nanoparticles (ION). An average of 269 $\pm$ 76 intravascular monocytes were detected as hypointense spots within the brain during a scan time of 2 h 44 min in healthy mice (Fig. 2b, c and supplemental video 1).

To further characterize motion patterns of *in vivo* detected cells by time-lapse MRI, cells were classified according to their spatial and temporal characteristics (Fig. 2c). 139 $\pm$ 35 cells ($\sim$52% of total detected cells) were observed in only 1 or 2 time frames, classified as short-term pattern. 73 $\pm$ 31 ($\sim$27%) cells were observed in the same voxel during longer observation times, classified as long-term short-range pattern. 58 $\pm$ 33 ($\sim$21%) cells were observed moving across several voxels, classified as long-term long-range pattern. For the latter, a motion velocity in the imaging plane of 0.19 $\pm$ 0.01 μm/s was calculated (Fig. 2d), corresponding to the expected average velocity of patrolling monocytes [5]. We used computer simulations with increasing velocity of artificial cells and verified that only slowly moving cells were detected by time-lapse MRI. Stationary cells and cells with velocities $<$ 1μm/s generated contrast in the simulated images, but faster moving cells were not detectable (Fig. 2e). The observed hypointense spots were mainly attributed to monocytes labelled by *in vivo* ION intravenous application. Flow cytometry analysis using fluorescent rhodamine-conjugated ION in LysM-GFP mice (GFP expression in myeloid cells, expression level dependent on cell type [15] showed that mainly monocytes are labelled by this *in vivo*

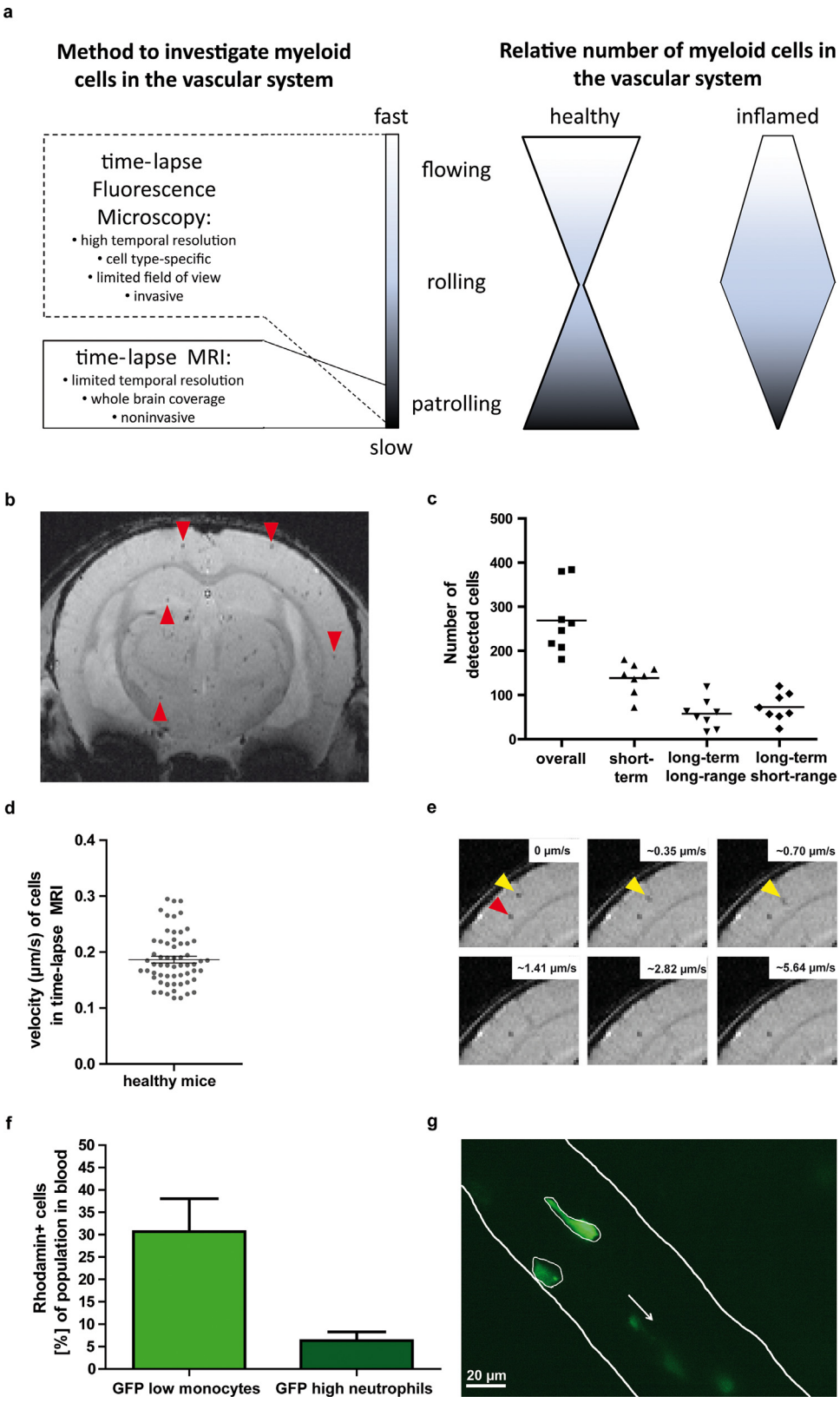

Figure 2. Resolving patrolling behaviour of monocytes a) Scheme illustrating specificity of applied imaging techniques for dynamic detection and tracking of single immune cells with regard to resolvable range of velocity (left panel). Inflammatory stimuli foster rolling behaviour of immune cells compared to the healthy state initiating the leucocyte adhesion molecule cascade. **b)** Exemplary slice of time-lapse MRI of a healthy mouse brain after *in vivo* cell labelling, showing multiple hypointense spots (some are highlighted by red arrowheads) representing labelled cells. Time-lapse MRI enables to track these cells along the time axis with whole brain coverage (supplementary video 1). **c)** Number of detected cells by time-lapse MRI with whole brain coverage in healthy mice (n = 8). In addition to total number of detected cells (overall), motion patterns were classified as short-term, long-term long-range, and long-term short-range patterns. **d)** In-plane velocity was calculated for cells with a long-term long-range pattern from time-lapse MRI data showing a mean velocity of 0.19 ± 0.01 μm/s. **e)** Computer simulations with increasing cell velocities showed that labelled cells with velocities beyond >1μm/s are not detectable by time-lapse MRI. For the simulations moving artificial cells (yellow arrowheads) which reproduced signal properties of real cells (red arrowhead) were overlaid with real *in vivo* time-lapse MRI data. **f)** Flow cytometry analysis of labelled monocytes from LysM-GFP mice. *In vivo* labelling with rhodamine-conjugated ION in n=7 mice showed, that mainly monocytes were labelled. GFP: green fluorescent protein. For details see also supplementary Figure 2. **g)** Intravital microscopy via a cranial window in LysM-GFP mice verified the presence of cells slower than 1 μm/s (see also supplementary video 2). Scale bar = 20 μm; the white arrow indicates the direction of blood flow.

approach (supplementary Figure 2). In detail, 30.7 ± 7.3% of monocytes but only 6.3 ± 1.9% of neutrophils were labelled (Fig. 2f). We therefore conclude that our time-lapse MRI protocol detects mainly slowly moving (patrolling) and stationary monocytes. Here, the long-term long-range pattern can be attributed to monocytes that patrol over distances beyond one voxel (> 100 μm). The short-term pattern represents cells that exert patrolling behaviour only for a short period of time (< 40 μm distance covered) and are therefore detected in one MRI voxel. The long-term short-range pattern represents cells that patrol a restricted area for longer times. For the latter, however, it cannot be excluded that they are confounded with stationary cells.

The presence of patrolling monocytes moving slower than 1μm/s, besides faster moving cells such as those that showed rolling behaviour or were flowing in the blood stream, was independently confirmed by intravital microscopic analysis (Fig. 2g and supplementary video 2).

3.2. Resolving patrolling monocytes under inflammatory stimuli

We next aimed to observe patrolling monocytes and their motion pattern following either peripheral or systemic inflammatory stimuli, to further characterize early immune responses.

3.2.1. Alteration of intravascular monocyte patrolling behaviour during the time course of inflammation

First, patrolling behaviour was observed along the time axis. After triggering peripheral inflammation, in a model of local pellet inflammation, we observed a significant decrease in the number of detected cells ($p<0.001$ [Welch-ANOVA], Fig. 3a), which was present in all motion pattern categories (all $p<0.001$ [Welch-ANOVA], supplementary figure 3a-c, supplementary table 1). Compared to healthy mice (269 ± 27), the number of detected cells slightly decreased at 24 h (253 ± 63) and 48 h (172± 16). At 72 h (144 ± 17) and 7 d (36 ± 6) post induction of inflammation the number of detected cells was significantly lower than in healthy mice ($p=0.023$ and $p<0.001$ [Games-Howell post-hoc test]). The same temporal evolution was observed for the short-term and long-term long-range pattern, while the long-term short-range pattern was significantly lower compared to healthy mice only at 7 d post inflammatory onset (supplementary figure 3 and table 1). Regarding the relative fraction of cells with specific motion patterns, the long-term short-range pattern was more frequently observed after 72 h (54.3 ± 3.6 %) than after 24 h (33.8 ± 3.0%, $p=0.002$ [Games-Howell post-hoc test]), 48 h (29.8 ± 3.3%, $p<0.001$ [Games-Howell post-hoc test]) or 30 d (18.4 ± 3.2 %, $p<0.001$ [Games-Howell post-hoc test]) as well as in control mice (26.5 ± 2.6%, $p<0.001$ [Games-Howell post-hoc test]; Fig. 3b, supplementary table 2). Meanwhile, the short-term and long-term long-range pattern were observed less frequently at 72 h after induction of the peripheral inflammation compared to the other time points and control mice (supplementary Fig. 3d, e). 30 d after the initial stimulus the peripheral inflammation was clinically healed, and the number of detected cells (329 ± 93) as well as their motion patterns restored to the level of healthy control mice (Fig. 3a, b and supplementary Fig. 3).

To further assess the timely evolution of early immune response, we used the CLP peritonitis model. With time-lapse MRI, we observed a decrease in detected cell numbers as soon as 2 h after sham (1440 ± 320, $p=0.001$ [rm-ANOVA with Bonferroni-adjusted post-hoc test], Fig. 3c, supplementary table 3) as well as after CLP surgery (1640 ± 316, but $p=0.061$ [rm-ANOVA with Bonferroni-adjusted post-hoc test], Fig. 3c) compared to baseline before surgery (2255 ± 311 for sham or 2533 ± 504 for CLP mice, respectively). In the CLP group the number of detected cells was significantly lower 2 h after surgery (1640 ± 316) compared to 0.5 h after surgery (2426 ± 316, $p=0.019$ [rm-ANOVA with Bonferroni-adjusted post-hoc test], Fig. 3c). Importantly, the time point 2h post-surgery is far ahead of the appearance of any symptoms (12 h) as well as of inevitable progress to severe sepsis (24 h). Regarding analysis of motion patterns, only the short-term pattern decreased 2 h after sham ($p=0.003$ [rm-ANOVA with Bonferroni-adjusted post-hoc test]) or CLP ($p=0.023$ [rm-ANOVA with Bonferroni-adjusted post-hoc test]) compared to baseline (supplementary Fig. 4 a-f and supplementary table 3). Long-term patrolling behaviour was observed more frequently 2 h after sham (57.3 ± 1.7%, $p=0.036$ [rm-ANOVA with Bonferroni-adjusted post-hoc test]) and after CLP surgery (66.6 ± 2.9%, $p=0.2$ [rm-ANOVA with Bonferroni-adjusted post-hoc test]) compared to baseline (51.6 ± 1.1% or 50.11 ± 3.1%, respectively; supplementary Fig. 4g, h). Here, the long-term short-range pattern was more common (supplementary table 4). IVM was in parallel performed in naïve, sham and CLP mice and confirmed presence of rhodamine-ION labelled cells (LysM-eGFP mouse model) in healthy mice (Fig. 3d). Patrolling monocytes with a velocity of <1 μm/s were observed in naïve, sham and CLP mice (Fig. 3e, f). Importantly, due to small field-of-view of IVM quantification of detected cells as performed for time-lapse MRI is not feasible in microscopy. On the other end of the velocity scale, where flowing and rolling patterns occur, IVM revealed a significant decrease in cell velocity in sham and CLP mice compared to control mice (Fig. 3g, h).

Taken together the number of patrolling monocytes tracked distant to the stimulus site by time-lapse MRI decreased significantly after an inflammatory stimulus and returned to baseline after clinical recovery. Changes were observed considerably earlier in a model of peritonitis (as early as 2 h) than in peripheral sterile inflammation (72 h). In both models, however, the detected cells showed a shift towards a more long-term short-range patrolling pattern upon inflammatory stimuli, which can be interpreted as an intensified patrolling behaviour of remaining cells.

3.2.2. Monocyte patrolling behaviour depends on type and intensity of inflammatory stimulus

We next aimed to investigate, if patrolling behaviour of monocytes is also dependent on the type and intensity of the inflammatory stimulus. Therefore, we first increased the inflammatory load in the peripheral inflammation model by increasing LPS dose (from 10 μg to 40 μg LPS). Compared to healthy mice less cells were detected, which was only significant, however, for the lower dose (10 μg: $p=0.027$ and 40 μg: $p=0.299$ [Games-Howell post-hoc test]; Fig. 4a). A significant decrease was similarly found for the long-term long-range patrolling pattern in the 10 μg LPS group ($p=0.036$ [Games-Howell post-hoc test]) and the 40 μg LPS group ($p=0.022$ [Games-Howell post-hoc test]), and for the short-term patrolling pattern in the 10 μg LPS group ($p=0.041$ [Games-Howell post-hoc test]) (supplementary Fig. 4a-c and supplementary table 1). Regarding the relative number of cells with specific motion patterns, significantly fewer cells showing a long-term long-range pattern were observed after a 10 μg LPS stimulus compared to healthy mice (12 ± 1.1% vs. 20 ± 2.9%, $p=0.021$ [Games-Howell post-hoc test], supplementary table 2). Following a 40 μg LPS stimulus, significantly more cells showing a long-term short-range pattern (43 ± 4.9% vs 26 ± 2.6%, $p=0.01$ [Games-Howell post-hoc test]) and significantly fewer cells showing a long-term long-range pattern (8 ± 0.8% vs 20 ± 2.9%, $p=0.002$ [Games-Howell post-hoc test]) were found (supplementary table 2). These data suggest that a stronger inflammatory stimulus causes a shift in patrolling behaviour from long-range towards long-term short-range patrolling.

In a second step, we modified the type of inflammatory stimulus to a primarily systemic stimulus and observed cells 48 h after induction of inflammation by bacteraemia using *S. aureus*. Time-lapse MRI detected significantly lower cell numbers in this bacteraemia model (102 ± 5) compared to healthy mice (269 ± 27, $p<0.001$ [Tukey post-hoc test], Fig. 4b). Cell numbers were not significantly different from the peripheral inflammation model at the same time point (172 ± 41, $p=0.169$ [Tukey post-hoc test]). To further study the observed

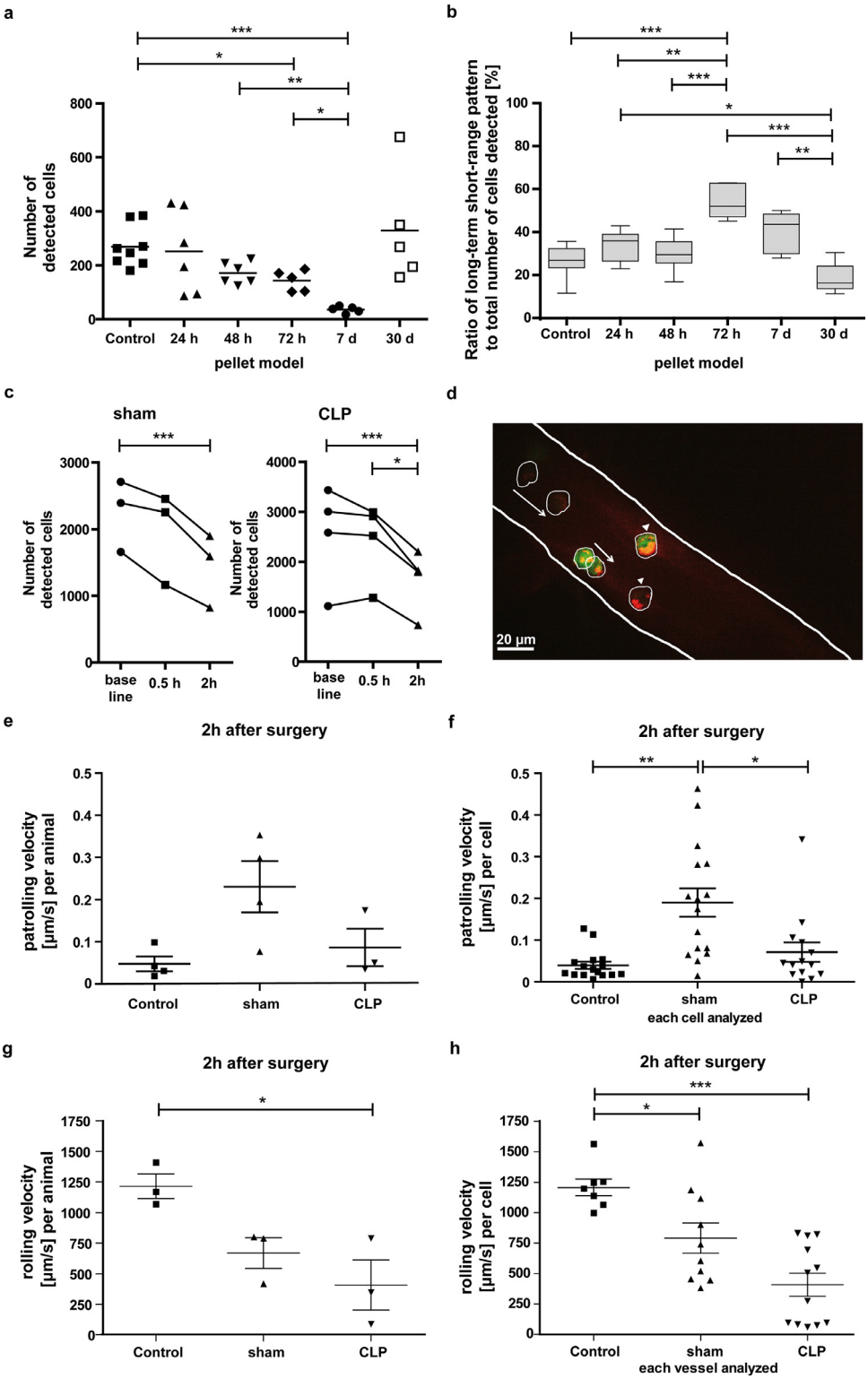

Figure 3. Alteration of intravascular monocyte patrolling behaviour is time-dependent a) Number of detected cells by time-lapse MRI at 5 time points after induction of a peripheral inflammation compared to control mice each 24 h after *in vivo* labelling of monocytes with ION. **b)** Ratio of cells with long-term short-range patrolling pattern to all cells detected at 5 time points after induction of a peripheral inflammation compared to control mice each 24h after *in vivo* labelling with ION. **c)** Number of detected cells by sequential time-lapse MRI prior to (baseline), 0.5 h and 2 h after sham (left panel) or CLP surgery (right panel) of LysM-GFP mice after *in vivo* labelling cells with rhodamine-ION**.** Detailed numbers and statistics can be found in supplementary table 1-4. **d)** IVM via cranial window of LysM-GFP mice confirmed intravascular presence of *in vivo* rhodamine-ION-labelled cells (white arrowheads indicate non-moving cells; white arrows indicate patrolling cells). As not all displayed cells were in the focus level and green fluorescence could not be depicted equally in this image, patrolling monocytes were framed. Scale bar = 20 μm. **e)** IVM analysis of patrolling velocity (μm/s) in Lys-GFP mice after sham or CLP surgery as well as in healthy control mice on a per animal (e) or **f)** per cell basis. **g)** IVM analysis of rolling velocity (μm/s) in LysM-GFP mice after sham or CLP surgery as well as in healthy control mice on a per animal (g) or **h)** per cell basis. $^{*}p<0.05$, $^{**}p<0.01$, $^{***}p<0.001$.

Table 1
Motion patterns of monocytes

Motion pattern	Motion pattern as defined by time-lapse MRI	Underlying motion behaviour
short-term short-range	cells detected in one or two consecutive time frames within the same voxel	short-range patrolling
short-term long-range	cells too fast to be detected by time-lapse MRI	flowing / rolling (>1μm/s)
long-term short-range	cells detected in three or more consecutive time frames within the same voxel	short-range patrolling / adherent
long-term long-range	cells detected in three or more consecutive time frames with observed motion in-plane or to a consecutive slice	long-range patrolling

modulation of intravascular monocyte patrolling behaviour in response to a systemic stimulus such as bacteraemia, we next modulated the intensity of the inflammatory stimulus in this model. We used either gram-positive *S. aureus* or gram-negative *E. coli*, each in a lower (10^5 colony forming units (CFU)) and a higher (10^7 CFU) dose.

For an injected dose of 10^5 CFU, the number of detected cells was significantly lower for both bacterial strains (*S. aureus*: 102 ± 5, p<0.001; *E. coli*: 62 ± 12, p<0.001 [Tukey post-hoc test]) than for healthy control mice (269 ± 27; Fig. 4c). Between the two strains no significant difference was found (supplementary table 5). Regarding motion patterns of detected cells, a significant decrease compared to control mice was observed for all motion patterns with both bacterial strains (supplementary Fig. 5d-f and supplementary table 5). We therefore conclude that low-dose bacteraemia leads to a lower number of monocytes with patrolling behaviour.

High dose bacteraemia with *S. aureus* also resulted in a reduced number of detected cells, as compared to healthy mice (136 ± 19 vs. 269 ± 27, p=0.006 [Games-Howell post-hoc test]; Fig. 4d). This decrease was observed for all motion patterns (supplementary Figure 5g-i and supplementary table 5). In contrast, high dose *E. coli* bacteraemia led to an increase in the number of detected cells (4882 ± 1210) as compared to healthy mice (269 ± 27, p=0.063 [Games-Howell post-hoc test], Fig. 4d). Here, all motion patterns were detected more frequently, although not reaching significance (supplementary Fig. 5g-i). However, the percentage of the long-term long-range patrolling cells was lower in high-dose *E. coli* bacteraemia diseased mice than in healthy mice (6.6 ± 0.9% vs. 20.4 ± 2.9%, p=0.008 [Tukey post-hoc test], supplementary Table 6), while it was higher for the long-term short-range pattern (45 ± 0.5% vs. 26 ± 2.6%, p=0.001 [Tukey post-hoc test])Comparing between strains, the long-term short-range pattern was more frequent in high-dose *E. coli* (45 ± 0.5%) than in *S. aureus* (27.5% ± 2.1%, p=0.003 [Tukey post-hoc test], supplementary table 6). Further, the short-term pattern was less frequent in high-dose *E. coli* (48 ± 0.7%) than in *S. aureus* (62 ± 2.0%, p=0.008 [Games-Howell post-hoc test]). We conclude that, under high dose *E. coli* bacteraemia monocytes shift towards a more stationary long-term patrolling behaviour.

To explain these seemingly paradoxical observations for the high dose *E. coli* bacteraemia model, we performed blood cell analyses to correlate MRI signal to total number of cells within the systemic circulation. In accordance with the MRI results, only the high dose *E. coli* model showed a tendency to higher numbers (not significant) of white blood cells (WBC) as compared to control mice (1.998 ± 0.576 $10^3/\mu$l vs. 1.340 ± 0.294 $10^3/\mu$l, p=0.618 [Tukey post-hoc test],

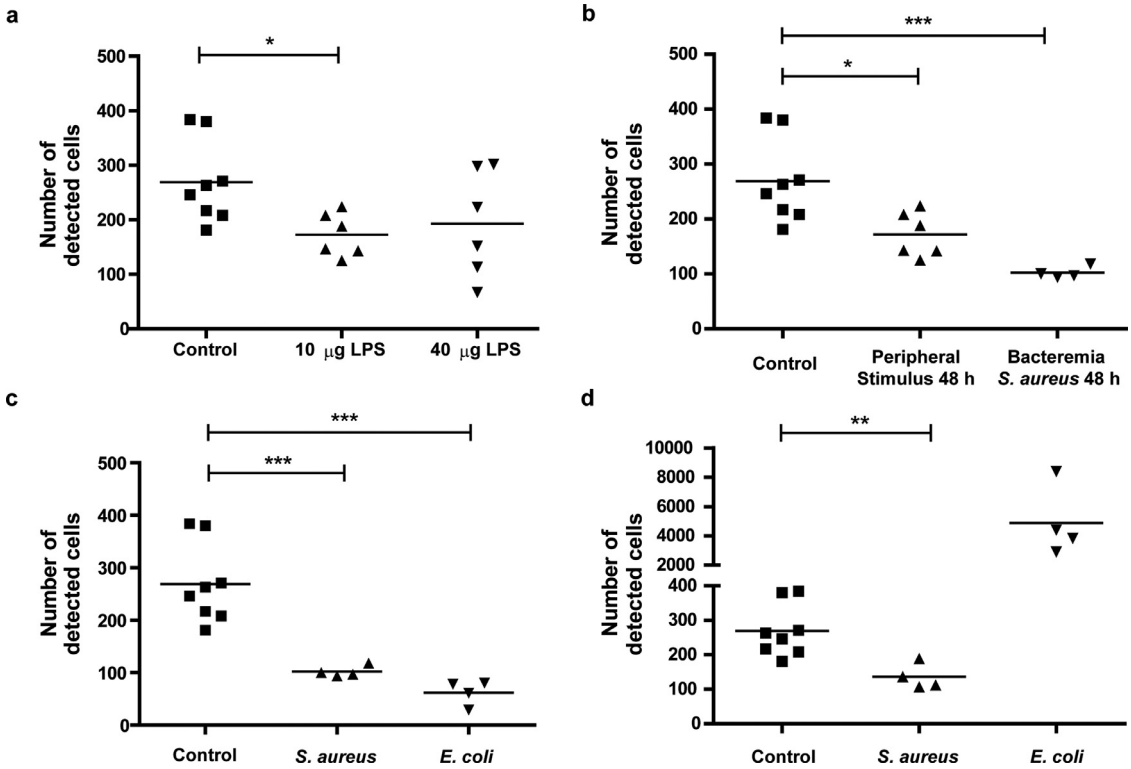

Figure 4. Alteration of monocyte patrolling behaviour depends on type and extent of inflammatory stimulus a) Number of detected cells by time-lapse MRI 48 h after induction of a peripheral inflammation with either 10 μg or 40 μg lipopolysaccharide (LPS) within the subcutaneous polyacrylamide-gel pellet compared to control mice, each 24 h after *in vivo* labelling with ION. **b)** Number of detected cells by time-lapse MRI 48 h after induction of a peripheral inflammation (10 μg LPS) or bacteraemia with *S. aureus* (low dose: 10^5 CFU) compared to control mice, each 24h after *in vivo* labelling with ION. **c)** Number of detected cells by time-lapse MRI 48 h after induction of low-dose bacteraemia with *S. aureus* or *E. coli* compared to control mice. **d)** Number of detected cells by time-lapse MRI 48 h after induction of high-dose bacteraemia with *S. aureus* or *E. coli* compared to control mice. Detailed numbers and statistics can be found in supplementary table 5-6. *p<0.05, **p<0.01, ***p<0.001.

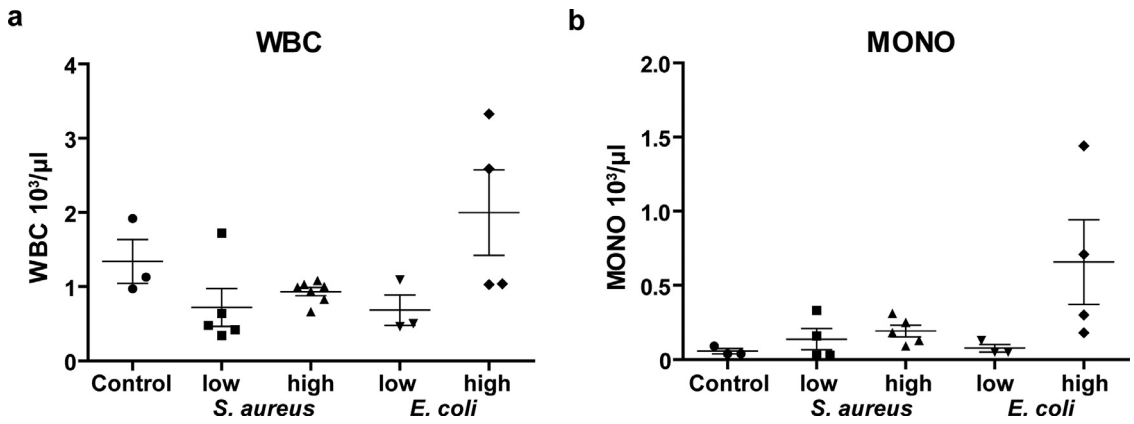

Figure 5. Blood count in bacteraemia model Blood samples obtained directly after time-lapse MRI showing number of **a)** white blood cells (WBC) and **b)** monocytes (mono) in the model of low-dose and high-dose bacteraemia compared to control mice. Blood samples in high-dose *E. coli* bacteraemia show a higher number of monocytes than in low-dose *E. coli* and *S. aureus* bacteraemia or control mice (at least n = 3 for each group).

Fig. 5a), while all other bacteraemia models showed a trend to lower (albeit not significant) number of WBC. In detail, the monocyte count revealed moderately increased numbers in all bacteraemia models, except for the high dose *E. coli* model, which showed a more than eleven-fold increase in monocytes compared to control mice (658 ± 284/μl vs. 57 ± 17/μl, p=0.081 [Tukey post-hoc test], Fig. 5b).

In summary, non-invasive time-lapse MRI revealed that monocyte motion patterns in the vascular system are altered by inflammatory stimuli. This alteration (i) is not a local effect, but can be detected distant from the affected tissue; (ii) is time dependent over the course of inflammation; (iii) is varying with type and intensity of the inflammatory stimulus; and (iv) disappears when the inflammation is clinically healed.

4. Discussion

Immune cells change their motion pattern upon inflammatory stimuli, initiating the leucocyte-adhesion cascade within the inflamed vascular bed [6]. It is known that immune cells also exhibit different motion patterns in health and disease, which especially holds true for non-classical monocytes screening the endothelium for pathogens. In this context, a patrolling behaviour of monocytes has been described with short- and long-range patterns [5]. Knowledge of patrolling monocytes and their motion patterns distant to the site of inflammation and the primarily affected vascular territory, lying beyond the limited field-of-view of IVM is scarce. Here, we show by using time-lapse MRI, that local as well as systemic intra- and extravascular inflammatory stimuli both modulate intravascular monocyte patrolling behaviour. Our data suggest, that altered motion patterns depend on the type, duration, and strength of the inflammatory trigger.

The complex response to inflammatory diseases by the innate and adaptive immune system [21] demands for *in vivo* methods to longitudinally study the fate of individual cells [5,22-24]. With regards to potential clinical translation non-invasive cell tracking, which avoids disrupting the integrity of the studied organism, is advantageous. Non-invasive methods other than MRI have detected single cells [23], but MRI with ION-labelling is superior regarding spatial resolution, anatomical correlation and abstinence of radiation or radioactive tracers [13,25]. Conventional ION-based non-invasive MRI cell tracking only provides a snap shot of labelled cells at confined locations and certain time points [26-28], but does not capture intravascular motion behaviour [11-14]. Instead, time-lapse MRI enables to monitor the actual dynamics of moving cells [9,10]. Here, we show that time-lapse MRI allows for the detection of slow movement, called patrolling, of single monocytes at a mean velocity of 0.19 ± 0.01 μm/s. This velocity is in line with previous studies on patrolling monocytes, which has been reported about 0.2 μm/s [5]. Of note, upon inflammatory stimuli monocytes initiate a rolling behaviour (40 μm/s or more) [5,7], which is beyond the detection window by time-lapse MRI [9]. The temporal resolution of time-lapse MRI thus discriminates between “non-stimulated” monocytes patrolling the vasculature and “stimulated” rolling monocytes. Consequently, in case of inflammatory stimuli the number of detected hypointense spots representing *in vivo* ION-labelled cells is reduced compared to the healthy state. Importantly, this holds also true for primary inflammatory diseases of the brain as previously shown for time-lapse MRI in the animal model of multiple sclerosis [9]. Further, this notion is in line with previous IVM studies as well as with the IVM data presented here. These show an increase in rolling behaviour upon a certain stimulus [5,7] with a lower fraction of cells that are either moving very fast (not detectable in the range of time-lapse MRI) or patrolling very slowly.

Accordingly, time-lapse MRI indicates the transition from intravascular monocyte patrolling to rolling by detecting lower numbers of labelled cells. Importantly, time-lapse MRI holds the advantages of non-invasiveness and whole organ coverage providing a field of view beyond IVM.

After peripheral local subcutaneous inflammation, time-lapse MRI revealed altered monocyte patrolling behaviour distant to the primary site of inflammation. During the course of inflammation, the number of patrolling cells decreased to a minimum at 72 h and 7 d, when inflammation is known to peak in this established model [16,18,29]. However, as observed in the CLP model, such a change in motion pattern can take place as early as 2 h after onset of the inflammatory stimulus representing the immediate systemic immune response distant to the affected vascular bed. Interestingly, for CLP and sham procedure a similar decrease in detected patrolling monocytes compared to baseline was observed 2h after surgery (36.1% for sham procedure and 35.3% for CLP procedure). In this model, septic symptoms of mice appear not earlier than 8-18h after surgery. Here, the observed decrease in patrolling cells may be more attributed to the impact of the surgery procedure rather than to the septic situation caused by intestinal germs infecting the peritoneal cave. However, the model shows that changes in systemic monocyte patrolling behaviour appear very early, illustrating the high sensitivity of time-lapse MRI for detecting this early immune response. As seen for the peripheral subcutaneous inflammation, monocyte dynamics also timely detected recovery from inflammatory disease. Thus, the number of patrolling cells detected by time-lapse MRI correlated with the current inflammatory status.

In our study a lower number of patrolling monocytes was observed upon inflammatory stimuli as compared to healthy state.

However, a higher fraction of these remaining patrolling cells was detected for longer periods than for a few time frames only. This long-term pattern was found particularly for cells that remained at the same position (short-range pattern) and less for moving cells (long-range pattern), suggesting that fewer patrolling monocytes patrol the endothelium more stationary after an inflammatory stimulus. Triggering rolling behaviour of immune cells along the endothelium is one of the initial steps of the leucocyte adhesion cascade, ultimately leading to cell extravasation into the target tissues [6]. Importantly, a short-term long-range MRI pattern represents rolling and is too fast to be detected by time-lapse MRI. In contrast, extravasated leucocytes are expected to have a more stationary motion pattern, most likely to be detectable by time-lapse MRI. In this context, high-dose *E. coli* injection led to an opposite pattern in time-lapse MRI compared to the other inflammatory stimuli. A higher number of cells remained at the same position over several time frames (long-term short-range behaviour). High-dose *E. coli* injection potentially triggered a septic response of the immune system with massive recruitment of monocytes from their reservoirs (such as bone marrow or spleen). In agreement, differential blood counts showed a higher number of monocytes in this situation compared to the other scenarios. This conception is in line with results from the first experiments evaluating time-lapse MRI upon stimulation by LPS, where a higher number of labelled cells were observed within the cerebral circulation [10]. This leads to the conclusion, that time-lapse MRI depicts both early activation of patrolling monocytes and advanced septic situations with massive immune cell activation, characterized by a different pattern and number of patrolling monocytes.

Of note, ION *in vivo* labelling by intravenous injection labels monocytes and, to a lesser extent other phagocytic cells like neutrophils [30]. Thus, a contribution of other cells to the observed time-lapse MRI motion pattern must be considered. Previous work with depletion of monocytes has shown that time-lapse signal can be mainly attributed to monocytes [9,10]. Additionally, *in vivo* labelling enables only to track a certain portion of all existing monocytes within the vasculature, potentially concealing the full picture of monocyte dynamics. In case specific labelling is needed, time-lapse MRI with *ex vivo* ION labelling of distinct cell types is feasible [9]. In the future, additionally T cell tracking may become feasible. However, current labelling approaches have not yet achieved sufficiently high iron concentrations in T cells for time-lapse MRI limiting its applications. Further, restrictions of ION-based MRI regarding signal specificity might be bypassed by using non-radioactive iron isotopes with low natural background [31]. A contribution of free ION to signal hypointensities detected by time-lapse MRI, appears highly unlikely. Free ION were recently shown to be cleared from the blood 24h after i.v. injection, the time when time-laose MRI was performed here [31]. Further, the small particle size of the administered ION, and the expected velocity of particles flowing with the blood stream renders detection of individual particles with the time-lapse MRI protocol virtually impossible. We therefore conclude that the observed signal alterations in time-lapse MRI originate from labelled cells. Detection of single monocytes is further corroborated by the presented flow cytometry and *in vitro* MRI data of micron-sized particles. Further support is provided by previous *in vivo* time-lapse MRI data with *ex vivo* labelled monocytes that showed similar signals as observed here [9].

In conclusion, we show that during inflammation monocyte patrolling behaviour is altered systemically depending on the type, strength and duration of the inflammatory stimulus. The occurrence of inflammation is indicated by a reduction of patrolling cells and a characteristic long-term short-range patrolling pattern, which resolves after recovery from inflammation. Time-lapse MRI, a non-invasive single-cell based dynamic imaging technique provides a dynamic spatial portray of intravascular immune cell patrolling behaviour.

We envision the technique to potentially gain relevance in diagnosing and monitoring inflammatory diseases under therapy. While this is currently limited to preclinical settings, future advances in magnet and detector technology might allow clinical applications in humans. With advances in contrast agents, time-lapse MRI is not necessarily restricted to phagocytosing cells. Therefore, the field of potential future applications may further expand from labelling other cell types to imaging other regions of interest as well as to other disease entities such as cancer and the associated tumour microenvironment.

Data Sharing Statement

The datasets generated during and/or analysed during the current study are available from the corresponding author on reasonable request.

Contributors

MM designed the study, developed and performed time-lapse MRI, analysed the data and wrote the manuscript.

FF designed the study, developed and performed time-lapse MRI and *ex vivo* experiments, analysed the data, edited the manuscript.

EW optimized time-lapse MRI protocol, performed and analysed *in vitro* measurements and time-lapse simulations, and edited the manuscript.

LZ performed surgical procedures, ex vivo experiments as well as intravital microscopy in the CLP model and edited the manuscript.

SN provided bacterial strains and advised data analysis of respective animal experiments.

LW developed time-lapse MRI and optimized animal handling during MRI, edited the manuscript.

CS performed and supervised handling of bacterial strains and according *ex vivo* experiments, edited the manuscript.

IF and AH performed and analysed time-lapse MRI data.

HB supervised intravital microscopy and CLP model and edited the manuscript.

MG and AHe advised data interpretation and edited the manuscript.

WH and AZ supervised study design and edited the manuscript.

MW designed the study, performed data analysis and wrote the manuscript.

CF designed the study, developed and supervised time-lapse MRI, analysed the data and wrote the manuscript.

MM, FF, MW and CF verify the underlying data of this manuscript.

All authors have read and approved the final version of the manuscript.

Declaration of Competing Interest

All authors declare no competing interests.

Acknowledgments

The authors thank Dr. Manfred Fobker, from the Laboratory Medicine Unit of the University Hospital Muenster for excellent support with mice blood analysis. This study was supported by the Deutsche Forschungsgemeinschaft (DFG, German Research Foundation) - CRC 1009 - 194468054 to AZ, CF and - CRC 1450 - 431460824 to MM, SN, HB, AZ, CF, the Joachim Herz Foundation (Add-on Fellowship for Interdisciplinary Life Sciences to MM), the Interdisciplinary Centre for Clinical Research (IZKF, core unit PIX) and the Medical Faculty of the University of Muenster (MEDK fellowship to FF and IF).

Supplementary materials

Supplementary material associated with this article can be found in the online version at doi:10.1016/j.ebiom.2021.103670.

References

[1] Singer M, Deutschman CS, Seymour CW, Shankar-Hari M, Annane D, Bauer M, et al. The Third International Consensus Definitions for Sepsis and Septic Shock (Sepsis-3). JAMA 2016;315(8):801–10.
[2] Grivennikov SI, Greten FR, Karin M. Immunity, inflammation, and cancer. Cell. 2010;140(6):883–99.
[3] Helfen A, Grosse Hokamp N, Geyer C, Heindel W, Bremer C, Vogl T, et al. Target-Specific Imaging of Cathepsin and S100A8/A9 Reflects Specific Features of Malignancy and Enables Estimation of Tumor Malignancy. Mol Imaging Biol 2020;22(1):66–72.
[4] Mantovani A, Allavena P, Sica A. Balkwill F. Cancer-related inflammation. Nature 2008;454(7203):436–44.
[5] Auffray C, Fogg D, Garfa M, Elain G, Join-Lambert O, Kayal S, et al. Monitoring of blood vessels and tissues by a population of monocytes with patrolling behavior. Science 2007;317(5838):666–70.
[6] Ley K, Laudanna C, Cybulsky MI, Nourshargh S. Getting to the site of inflammation: the leukocyte adhesion cascade updated. Nat Rev Immunol 2007;7(9):678–89.
[7] Schneider CA, Figueroa Velez DX, Azevedo R, Hoover EM, Tran CJ, Lo C, et al. Imaging the dynamic recruitment of monocytes to the blood-brain barrier and specific brain regions during Toxoplasma gondii infection. Proc Natl Acad Sci U S A 2019;116(49):24796–807.
[8] Karreman MA, Hyenne V, Schwab Y, Goetz JG. Intravital Correlative Microscopy: Imaging Life at the Nanoscale. Trends in cell biology 2016;26(11):848–63.
[9] Masthoff M, Gran S, Zhang X, Wachsmuth L, Bietenbeck M, Helfen A, et al. Temporal window for detection of inflammatory disease using dynamic cell tracking with time-lapse MRI. Sci Rep 2018;8(1):9563.
[10] Mori Y, Chen T, Fujisawa T, Kobashi S, Ohno K, Yoshida S, et al. From cartoon to real time MRI: in vivo monitoring of phagocyte migration in mouse brain. Sci Rep 2014;4:6997.
[11] Dodd SJ, Williams M, Suhan JP, Williams DS, Koretsky AP, Ho C. Detection of single mammalian cells by high-resolution magnetic resonance imaging. Biophysical journal 1999;76(1 Pt 1):103–9.
[12] Hinds KA, Hill JM, Shapiro EM, Laukkanen MO, Silva AC, Combs CA, et al. Highly efficient endosomal labeling of progenitor and stem cells with large magnetic particles allows magnetic resonance imaging of single cells. Blood 2003;102(3):867–72.
[13] Shapiro EM, Sharer K, Skrtic S, Koretsky AP. In vivo detection of single cells by MRI. Magnetic resonance in medicine 2006;55(2):242–9.
[14] Shapiro EM, Skrtic S, Sharer K, Hill JM, Dunbar CE, Koretsky AP. MRI detection of single particles for cellular imaging. Proc Natl Acad Sci U S A 2004;101(30):10901–6.
[15] Faust N, Varas F, Kelly LM, Heck S, Graf T. Insertion of enhanced green fluorescent protein into the lysozyme gene creates mice with green fluorescent granulocytes and macrophages. Blood 2000;96(2):719–26.
[16] Eisenblatter M, Ehrchen J, Varga G, Sunderkotter C, Heindel W, Roth J, et al. In vivo optical imaging of cellular inflammatory response in granuloma formation using fluorescence-labeled macrophages. Journal of nuclear medicine: official publication, Society of Nuclear Medicine. 2009;50(10):1676–82.
[17] Schmidt R, Nippe N, Strobel K, Masthoff M, Reifschneider O, Castelli DD, et al. Highly shifted proton MR imaging: cell tracking by using direct detection of paramagnetic compounds. Radiology 2014;272(3):785–95.
[18] von Stebut E, Metz M, Milon G, Knop J, Maurer M. Early macrophage influx to sites of cutaneous granuloma formation is dependent on MIP-1alpha /beta released from neutrophils recruited by mast cell-derived TNFalpha. Blood 2003;101(1):210–5.
[19] Toscano MG, Ganea D, Gamero AM. Cecal ligation puncture procedure. J Vis Exp 2011(51).
[20] Jenne CN, Wong CH, Petri B, Kubes P. The use of spinning-disk confocal microscopy for the intravital analysis of platelet dynamics in response to systemic and local inflammation. PLoS One 2011;6(9):e25109.
[21] Hemmer B, Kerschensteiner M, Korn T. Role of the innate and adaptive immune responses in the course of multiple sclerosis. The Lancet Neurology 2015;14(4):406–19.
[22] Greenwood J, Heasman SJ, Alvarez JI, Prat A, Lyck R, Engelhardt B. Review: leucocyte-endothelial cell crosstalk at the blood-brain barrier: a prerequisite for successful immune cell entry to the brain. Neuropathology and applied neurobiology 2011;37(1):24–39.
[23] Jung KO, Kim TJ, Yu JH, Rhee S, Zhao W, Ha B, et al. Whole-body tracking of single cells via positron emission tomography. Nat Biomed Eng 2020;4(8):835–44.
[24] Kirschbaum K, Sonner JK, Zeller MW, Deumelandt K, Bode J, Sharma R, et al. In vivo nanoparticle imaging of innate immune cells can serve as a marker of disease severity in a model of multiple sclerosis. Proc Natl Acad Sci U S A 2016;113(46):13227–32.
[25] Bulte JW, Kraitchman DL. Iron oxide MR contrast agents for molecular and cellular imaging. NMR in biomedicine 2004;17(7):484–99.
[26] Amsalem Y, Mardor Y, Feinberg MS, Landa N, Miller L, Daniels D, et al. Iron-oxide labeling and outcome of transplanted mesenchymal stem cells in the infarcted myocardium. Circulation 2007;116(11 Suppl):I38–45.
[27] Hoehn M, Kustermann E, Blunk J, Wiedermann D, Trapp T, Wecker S, et al. Monitoring of implanted stem cell migration in vivo: a highly resolved in vivo magnetic resonance imaging investigation of experimental stroke in rat. Proc Natl Acad Sci U S A 2002;99(25):16267–72.
[28] Lewin M, Carlesso N, Tung CH, Tang XW, Cory D, Scadden DT, et al. Tat peptide-derivatized magnetic nanoparticles allow in vivo tracking and recovery of progenitor cells. Nature biotechnology 2000;18(4):410–4.
[29] Fauve RM, Jusforgues H, Hevin B. Maintenance of granuloma macrophages in serum-free medium. Journal of immunological methods 1983;64(3):345–51.
[30] Korchinski DJ, Taha M, Yang R, Nathoo N, Dunn JF. Iron Oxide as an MRI Contrast Agent for Cell Tracking. Magnetic resonance insights 2015;8(Suppl 1):15–29.
[31] Masthoff M, Buchholz R, Beuker A, Wachsmuth L, Kraupner A, Albers F, et al. Introducing Specificity to Iron Oxide Nanoparticle Imaging by Combining (57)Fe-Based MRI and Mass Spectrometry. Nano Lett 2019;19(11):7908–17.